Streich, R., Becken, M., Matzander, U., Ritter, O. (2011): Strategies for land-based controlled-source electromagnetic surveying in high-noise regions. - The Leading Edge, 30, 10, 1174-1181

DOI: 10.1190/1.3657078

Strategies for land-based controlled-source electromagnetic surveying in high-noise regions

Rita Streich*, GFZ German Research Centre for Geosciences and Potsdam University

Michael Becken, University of Münster

Ulrich Matzander, Metronix

Oliver Ritter, GFZ German Research Centre for Geosciences

*corresponding author: rstreich@gfz-potsdam.de

Whereas marine controlled-source electromagnetic (CSEM) has become an established exploration tool in the hydrocarbon industry over the last decade, this is not the case for land-based CSEM. A possible reason is the perception that electromagnetic field energy traveling through air masks target responses much more than for marine surveys in which the "air wave" energy is attenuated by the conductive water. Various strategies for mitigating air-wave effects have been proposed recently (Løseth, Amundsen and Jenssen 2010, Chen and Alumbaugh 2011). In this contribution, we focus on other problems limiting the use of land-based CSEM. These include logistical and technical challenges related to high-power current transmission, and the high levels of cultural electromagnetic noise typical of target areas located in populated regions.

To tackle these challenges, we use a newly developed three-phase transmitter that allows collecting land CSEM data efficiently. By transmitting three-phase currents, multi-polarization data can be acquired without having to redeploy the transmitter at orthogonal orientations. This reduces the logistical effort of land CSEM data acquisition and, at the same time, improves subsurface illumination. We also introduce concepts for data processing. Because the land CSEM source is stationary, we can improve signal-to-noise ratios by time-domain stacking, and take advantage of the three-phase currents by adopting stochastic methods of transfer function estimation from passive magnetotellurics. Data examples from a survey carried out in late 2010 at the CO_2 injection test site in Ketzin, Germany, demonstrate that the combination of these concepts provides interpretable data even in very high-noise regions.

A three-phase CSEM transmitter

The three-phase transmitter is depicted in Figure 1. The entire system is powered by a standard 400 V generator that supplies three-phase, 50 Hz alternating currents (Figure 1a). These currents are fed into a programmable high-voltage, high-current signal generator (Figure 1b). Three grounded electrodes transmit the source signal into the subsurface (Figure 1c). For safety reasons, the power generator and signal generator are galvanically separated by a transformer. The signal generator

directly utilizes the three-phase current supplied by the generator. It rectifies the 50 (or 60) Hz, 400 V sinusoidal input currents to DC currents at a voltage of ~566 V. The DC voltage is switched by an arrangement of power semiconductors at a constant GPS-stabilized high frequency. The pulse width of the switching frequency is modulated to generate the desired CSEM source waveform and amplitude. This allows us to create a wide range of waveforms such as square waves, sine waves, or pseudo-random binary sequences (PRBS).

The overall source strength is determined by the length of the grounded electric sources and the current amplitudes. Typically, we use electrode cables about 1 km long, somewhat longer than most marine CSEM sources. However, the source length is limited by practical considerations. To maximize the source currents, according to Ohm's law ($I = U/R$, with voltage U and resistance R), we require high voltages and low coupling resistances between the electrodes and the ground. For practical and safety reasons, we keep the voltage between each pair of electrodes fixed to the value of 400 V*$\sqrt{2}$=566 V; this is the voltage supplied by standard power generators. We can then estimate the coupling resistances required. For example, to achieve currents of 40 A (the nominal maximum supported by our transmitter), the sum of resistances along the transmitter cables and electrodes should not exceed 14 Ω. For 2 km of copper cables having a total resistance of 2 Ω, the coupling resistance per electrode should thus be less than 6 Ω.

To achieve such low resistances, we use steel rods forced into the ground to depths of a few meters using a hand-held pneumatic hammer (Figure 1c). For all measurements carried out in central Germany to date, mainly in sandy soils, we obtained coupling resistances of 5 – 10 Ω for electrode depths between 4 and 11 m. Typically, coupling resistances drop rapidly as soon as the water table or a clay-rich soil layer is reached.

The currents on the three electrodes are phase-shifted to each other by 120°. The current I_k on electrode *k* can be written as

$$I_k = I_0 * \cos(k * 120° + \varphi),$$

where I_0 is the time-dependent source waveform and φ is a polarization angle that determines the distribution of the currents on the three electrodes. We generate multi-polarization fields for a fixed transmitter geometry simply by electronically adjusting the polarization angle. This allows for uniform subsurface illumination at much lower field effort than would be required with standard dipole transmitters. For every source polarization, the amplitude of the CSEM source field is very low within certain azimuth ranges from the source. By using several polarizations, we ensure that fields of measurable amplitude are generated at all azimuths.

Land CSEM survey at the Ketzin CO_2 storage site

We recently carried out a land CSEM survey across the CO_2 injection test site in Ketzin, Germany. At this site, CO_2 is being injected into an Upper Triassic sandstone aquifer at a depth of ~635 – 650 m, near the top of an anticline (Förster, et al. 2009). The CSEM survey had the goals of (i) demonstrating the feasibility of land CSEM in terms of field logistics and achievable data quality and (ii) resolving subsurface electrical resistivity in a wider region around the injection well than is currently being monitored (Schmidt-Hattenberger, Bergmann, et al. 2011).

We deployed 39 five-component receiver stations along an approximately N-S directed profile perpendicular to the trend of the main anticline structure (Figure 2), with an average receiver spacing of 270 m. We favored the line geometry over a sparse 3D layout because the dense receiver spacing allowed us better to observe the spatial decay of the EM fields. Each receiver measured the horizontal components of the electric field using 60-m long electrode dipoles, and three components of the magnetic field using induction coil magnetometers. The receivers were recording continuously, thus providing CSEM data and, in addition, passive magnetotelluric data at transmitter-off times.

While the receivers remained stationary throughout the experiment, the transmitter was set up at eight locations along and laterally offset from the receiver line (Figure 2). In theory, optimum uniform azimuthal distribution of CSEM source fields would be achieved by arranging the three transmitter electrodes in an equilateral triangle with the generator in the center, and then injecting

source currents at multiple polarizations. However, a specific layout is not required for operating the transmitter. Taking advantage of this flexibility, and adhering to the local field conditions, most transmitter cables were laid out along vehicle-accessible tracks in approximately L- or T-shaped geometries (Figure 2). This still provides reasonable subsurface coverage from multi-polarization source currents. The exact source geometries were recorded by GPS and are taken into account precisely in data processing and inversion.

We aimed at reaching a depth penetration of approximately 1 km, down to the flanks of the anticline of the CO_2-bearing formation and underneath the CO_2-bearing layer. To achieve this, we chose source signal frequencies between 1/64 Hz and 64 Hz, based on modeling studies carried out prior to the survey (Streich, Becken and Ritter 2010). The collection of multi-polarization data at a range of source frequencies and sufficient numbers of stacks for noise reduction required current injection times of 12 – 14 hours at each transmitter location.

Field operations required at least six to seven crew members at any time. A total of more than 20 people, scientists, students and technicians, were involved in the field work. Two one- or two-person teams were responsible for servicing each receiver (battery change, data retrieval, check for proper operation) about every other day. Setting up a transmitter required a two-people team and about half a day for deploying the electrodes, and another team of at least two people, depending on local conditions, for laying out the transmitter cables. Operating the transmitter required one person controlling and monitoring current injection and, depending on visibility of the cable tracks, at least two people guarding the electrodes and cables continuously.

Processing approaches

Examples of transmitted currents and received signals are shown in Figures 3 and 4. Because of the 120° phase shifts between the three currents, their sum is zero at all times (Figure 3a). For the 0.25-Hz signal shown, odd harmonics are recognizable up to the maximum frequency recorded. Pseudo-random binary sequences, which have a flat spectrum over a wide frequency range, were

also generated (Figure 3c). At receiver locations near the source, the recorded data closely resembles the source waveform (Figure 4a). The CSEM signal is clearly recognizable to offsets up to a few kilometers, yet increasingly overlain by noise (Figure 4b). At far offsets, the source signal is not directly visible in the raw data (Figure 4c).

Unfortunately, but typically for Germany or central Europe, several sources of very strong cultural noise were present in the survey area. The Ketzin site formerly hosted a facility for seasonal storage of natural gas (at shallower depth than present CO_2 injection). Accordingly, a network of gas pipelines is centered at the injection site. Some pipelines are still in use and maintained using an impressed-current cathodic protection system. In addition, a biogas plant and a transformer station are located next to the injection site. Several high-voltage power lines cross-cut the survey area, and a large array of wind power plants is located in the northeastern part of the area, with wind turbines present less than 200 m from the four northernmost receivers. Consequently, noise reduction is crucial for obtaining usable data.

To extract the signal from data dominated by noise (as in Figure 4c), we first stack the data in the time domain. In contrast to marine CSEM surveys, this is possible here because the source does not move. The examples of square-wave and PRBS signals displayed in Figure 5 demonstrate the effectiveness of time-domain stacking. A small number of time windows that contain the largest positive and negative amplitudes are removed as outliers using an alpha-trimmed mean procedure (Huber 1981; gray lines in Figures 5a and c). Summing the remaining time windows (blue lines in Figures 5a and c) results in traces in which the CSEM signals can be clearly recognized (red lines in Figure 5). The amplitude levels of both the square-wave and PRBS stacked traces are about ten times lower than those of the individual time windows. Stacking effectively removed time-variable noise. Persistent strong pipeline currents at a highly stable 15-s period could also be separated from the CSEM source signals by ensuring that CSEM signal periods differed from the noise period and its harmonics, and data were stacked over window lengths that were not multiples of the noise period.

Further noise reduction can be achieved by combining data from different source currents. This effectively requires normalization by the source current. Because the data contain the influence of three different currents from the three electrodes, simple normalization (i.e., deconvolution of the current) is not possible. Instead, we adopt the concept of transfer functions, which is well-known in magnetotelluric data processing (Berdichevsky and Dmitriev 2008) and more generally applicable to EM signals generated by a limited number of sources (Egbert 1997, Li and Pedersen 1991) Using this concept, we can write any electric or magnetic field component *F* in frequency domain as

$$F = (G_{F,13} \quad G_{F,23}) \begin{pmatrix} I_1 \\ I_2 \end{pmatrix}.$$

Here, I_1 and I_2 can be any two of the source currents and $G_{F,13}$ and $G_{F,23}$ are the corresponding transfer functions (the frequency dependency of all quantities is omitted). The third current does not appear in this expression because it is linearly dependent on the others, but (as indicated by the last index of *G*) its influence is implicitly included in the transfer functions *G*. These transfer functions are similar to Green's functions; they contain the desired information on subsurface resistivity, but in addition, they depend on the source geometry. Using the above expression, and considering the Fourier transforms of different stacked traces to be different samples of the field component *F*, we use robust statistical techniques to estimate the transfer functions *G* (Huber 1981, Egbert and Livelybrooks 1996, Weckmann, Magunia and Ritter 2005).

We apply robust iterative weighted least-squares averaging over data from different source currents. In addition to data from different source polarizations, the least-squares approach allows us to join data from different source waveforms and different source fundamental frequencies. For each fundamental frequency, we use a frequency band of about two decades, up to a maximum of 200 Hz. Due to the diffusive nature of electromagnetic fields, the response functions have to vary smoothly with frequency (Larsen, et al. 1996). Accordingly, we also average over the spectral peaks within narrow frequency bands.

Examples of resulting transfer functions are displayed in Figure 6. The transfer functions vary smoothly with frequency, as they should do, and their amplitudes decay as expected with distance from the source. They are also consistent in amplitude and phase with synthetic transfer functions computed using the exact source-receiver geometry (Streich and Becken 2011) and a 1D layered electrical conductivity model. The 1D responses were computed for a model used in previous synthetic studies on CSEM feasibility at the site (Streich, Becken and Ritter 2010) and are only displayed for rough comparison; data fit has not yet been attempted.

The obtained transfer functions and their space-frequency behavior are consistent over the entire profile, both for the electric and magnetic field (Figure 7). Poor data at a few stations can be explained by too close proximity to noise sources. As examples, the three stations with poorly determined Hx transfer functions at 7 and 9 km (Figure 7b) were located within 100 m from major power lines, and the stations with poor Ey at 5 km were located literally next to a transformer station. This demonstrates that reasonable data quality could generally be achieved despite the high level of cultural noise, but not for receivers located too close to major noise sources. Fortunately, the noise did not deteriorate all field components equally. At the receivers with poor Hx transfer function estimates in Figure 7, the Ey transfer functions are of reasonable quality and vice versa.

Conclusions

A land CSEM survey conducted in the high-noise area near the Ketzin CO_2 injection site demonstrates that land CSEM is feasible and can provide data of reasonable quality even in regions plagued by high levels of cultural noise. The combination of a new three-phase transmitter with novel processing strategies adapted from magnetotelluric data processing was key for the successful retrieval of the CSEM data from raw signal vastly dominated by cultural noise. The three-phase transmitter has proven to be advantageous in that it provides good subsurface coverage while allowing for flexible field layouts. Compared to standard dipole transmitters, the three-phase source reduces significantly the field effort required for collecting multi-polarization data.

For data processing, we take advantage of the three-phase current by adopting principles of transfer function estimation known from passive magnetotellurics. This allows us to combine data from different source polarizations and waveforms. In addition, we exploit a range of possibilities not available for marine CSEM data that are acquired with towed sources and, typically, only one or two different source periods. Stationary land CSEM sources and highly stable source signals allow us to stack the data over long transmission times, and spectral peaks can be evaluated over wide frequency ranges and averaged within narrow frequency bands for further noise reduction. Time- and frequency-domain stacking and stochastic approaches compensate, to some extent, for the considerably smaller number of source points, lower source power, and generally high noise levels in land CSEM compared to the marine case.

The primary rationale for using CSEM, i.e., its ability to discriminate between different pore fluids where subsurface structure is known, is the same on land as off-shore. This work indicates possibilities for dealing with some of the specific problems hindering wider use of land CSEM to date which are cheap and easy to implement. It may thus contribute to increasing the use of land CSEM in the future.

References

Berdichevsky, M. N., and V. I. Dmitriev. *Models and methods of magnetotellurics.* Heidelberg: Springer, 2008.

Chen, J., and D. L. Alumbaugh. "Three methods for mitigating airwaves in shallow water marine controlled-source electromagnetic data." *Geophysics* 76, no. 2 (2011): F89-F99.

Egbert, G. D. "Robust multiple-station magnetotelluric data processing." *Geophysical Journal International* 130 (1997): 475-496.

Egbert, G. D., and D. W. Livelybrooks. "Single station magnetotelluric impedance estimation: Coherence weighting and the regression M-estimate." *Geophysics* 61, no. 4 (1996): 964-970.

Förster, A., R. Giese, C. Juhlin, B. Norden, N. Springer, and CO2SINK Group. "The geology of the CO2SINK site: From regional scale to laboratory scale." *Energy Procedia* 1 (2009): 2911-2918.

Holmes, D. G., and T. A. Lipp. *Pulse Width Modulation for Power Converters: Principles and Practice.* Wiley-IEEE Press, 2003.

Huber, Peter J. *Robust statistics.* New York: Wiley, 1981.

Larsen, J. C., R. L. Mackie, A. Manzella, A. Fiordelisi, and S. Rieven. "Robust smooth magnetotelluric transfer functions." *Geophysical Journal International* 124 (1996): 801-819.

Li, X., and L. B. Pedersen. "Controlled source tensor magnetotellurics." *Geophysics* 56, no. 9 (1991): 1456-1461.

Løseth, L. O., L. Amundsen, and A. J. K. Jenssen. "A solution to the airwave-removal problem in shallow-water marine EM." *Geophysics* 75, no. 5 (2010): A37-A42.

Schmidt-Hattenberger, C., et al. "Application of a vertical electrical resistivity array (VERA) for monitoring CO2 migration at the Ketzin site: First performance evaluation." *Energy Procedia* 4 (2011): 3363-3370.

Streich, R., and M. Becken. "Electromagnetic fields generated by finite-length wire sources: comparison with point dipole solutions." *Geophysical Prospecting* 59 (2011): 361-374.

Streich, R., M. Becken, and O. Ritter. "Imaging of CO2 storage sites, geothermal reservoirs, and gas shales using controlled-source magnetotellurics: Modeling studies." *Geochemistry* 70 S3 (2010): 63-75.

Weckmann, U., A. Magunia, and O. Ritter. "Effective noise separation for magnetotelluric single site data processing using a frequency domain selection scheme." *Geophysical Journal International* 161 (2005): 635-652.

Acknowledgements

We are grateful to more than twenty members of the GFZ MT group and students for help with the field work, Metronix for providing the CSEM transmitter, and land owners for granting us access to their property. The receiver equipment was provided by the Geophysical Instrument Pool Potsdam (GIPP). The work was funded by the German Federal Ministry of Education and Research (BMBF) within the framework of the GeoEn project.

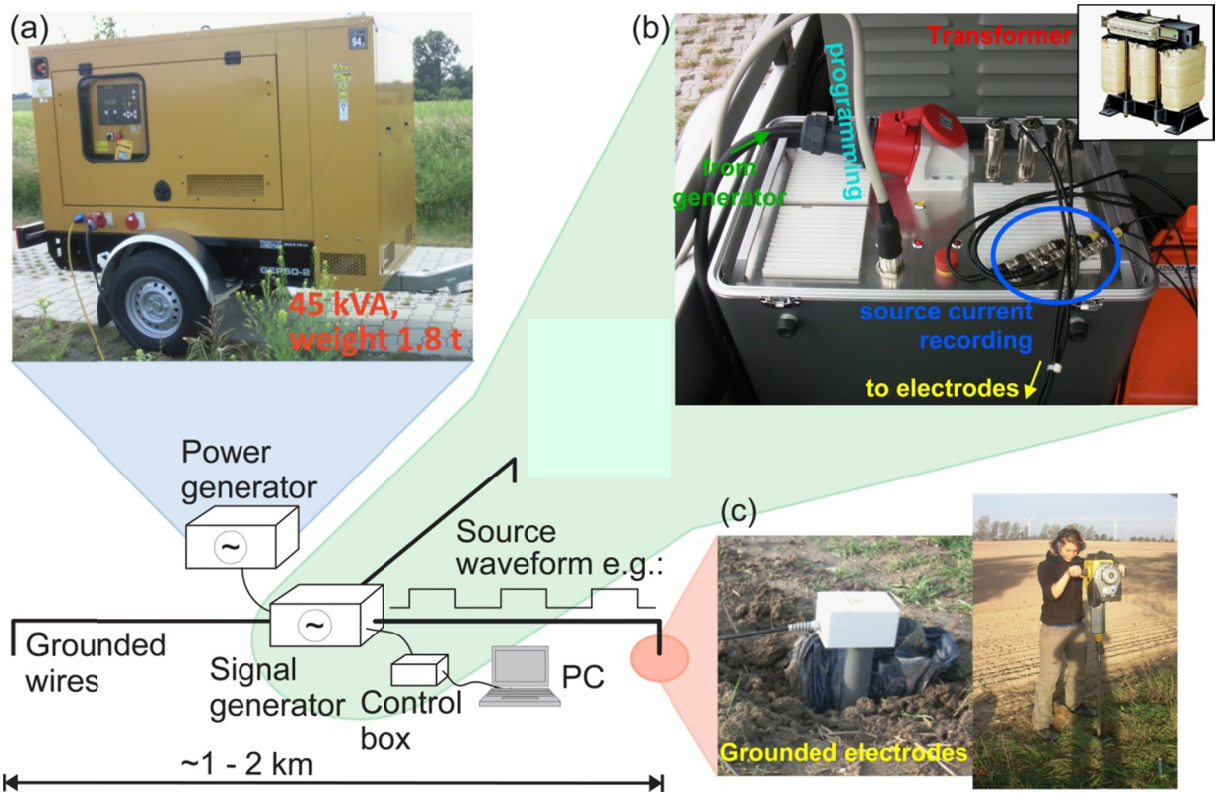

Figure 1: Principle sketch and field setup of the three-phase land CSEM transmitter, consisting of (a) a three-phase power generator, (b) a high-power, high-voltage programmable signal generator, and (c) grounded steel electrodes.

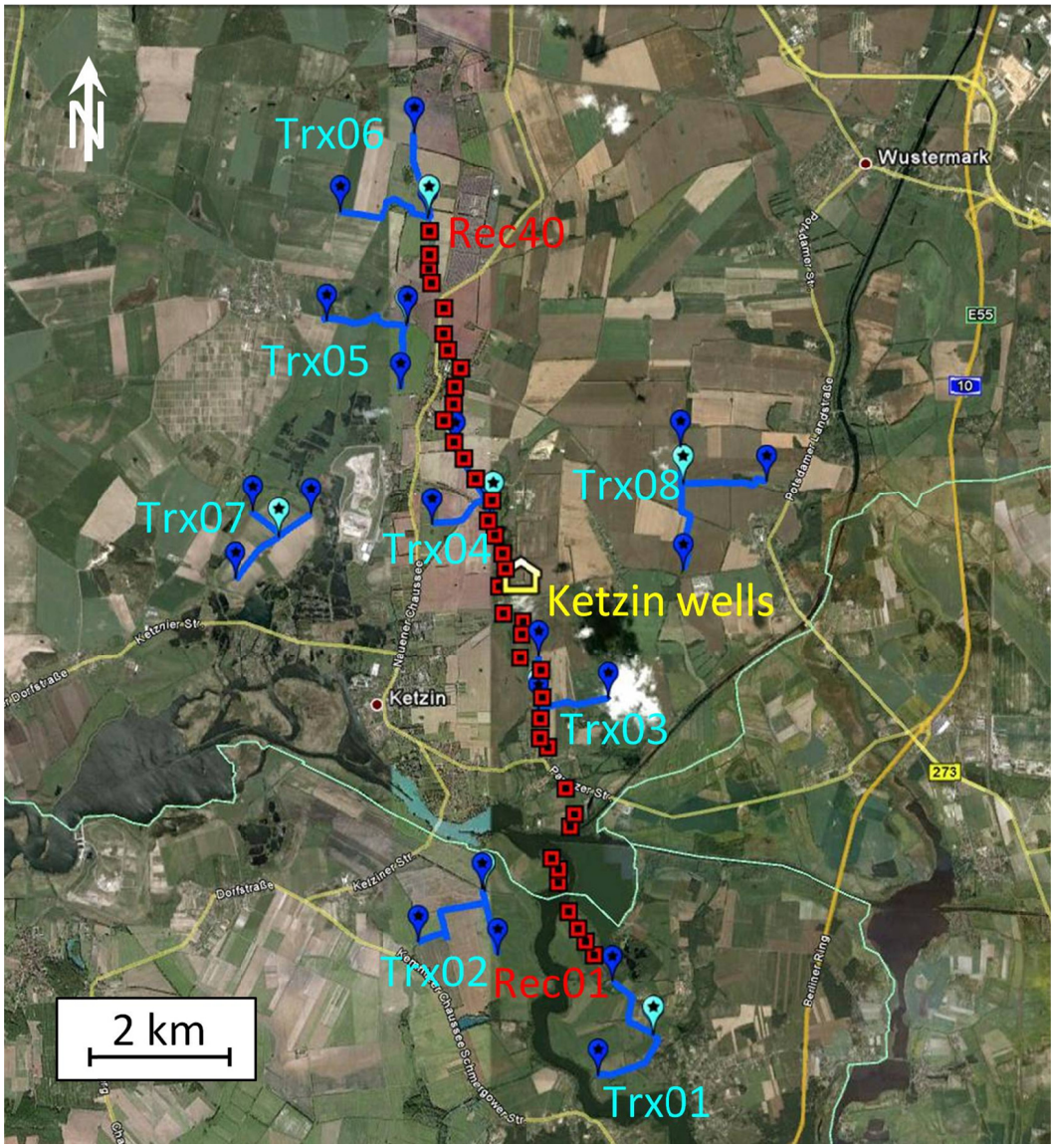

Figure 2: Geometry of the land CSEM demonstration survey at the Ketzin CO_2 injection site. Red squares indicate receivers, light blue dots indicate source generator locations and dark blue lines and dots indicate transmitter cables and electrodes. The CO_2 injection and monitoring wells are located in the center of the survey area.

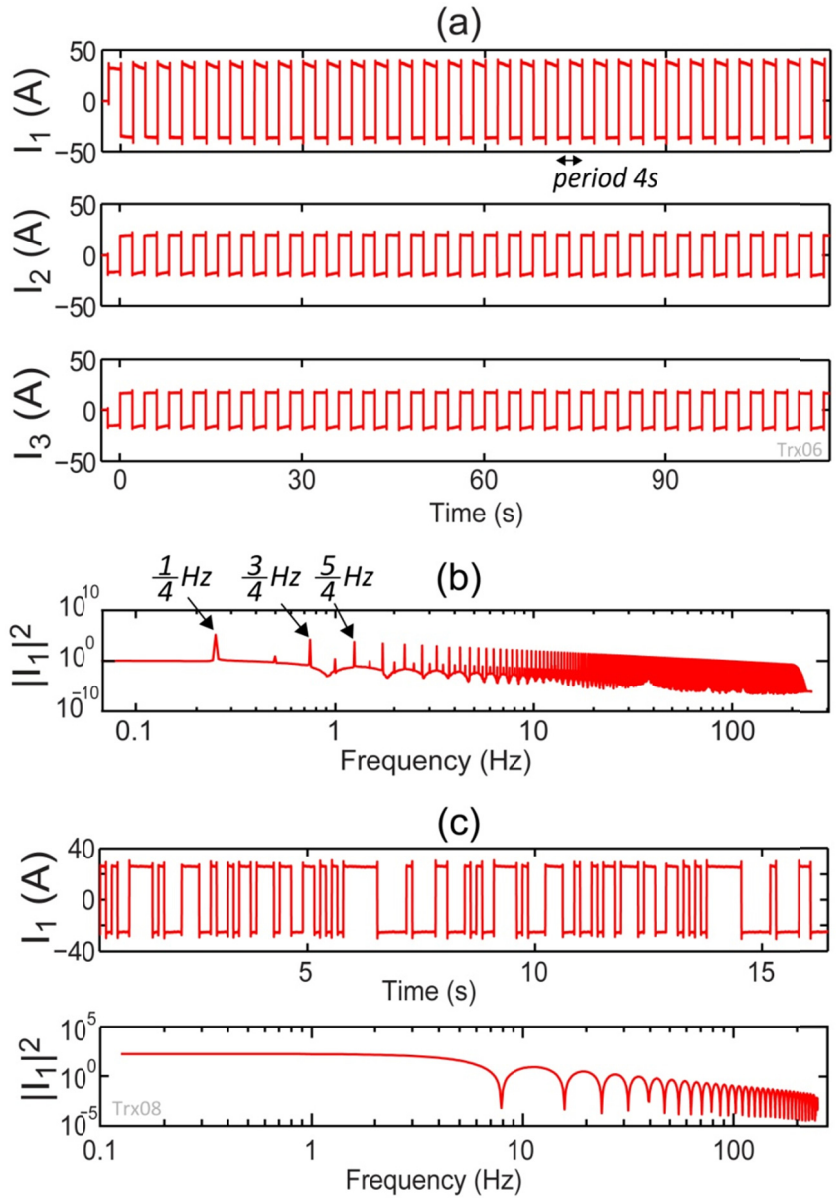

Figure 3: (a) Examples of square-wave source currents injected through the three source electrodes. Current amplitudes are nearly 40 A and the three currents sum up to zero. (b) Power spectrum for current I_1, showing well-defined peaks at the fundamental frequency and odd harmonics up to the Nyquist frequency of the recording device. (c) Example of a PRBS signal having a nearly flat spectrum over a wide frequency range.

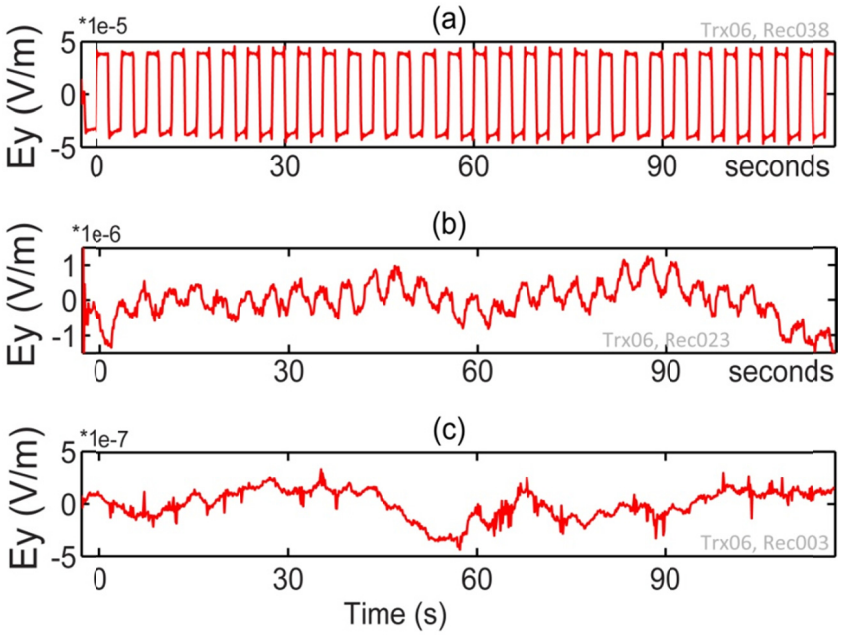

Figure 4: Examples of recorded electric field data for the source current displayed in Figure 3a and receivers located (a) 0.75 km, (b) 5 km and (c) 10.5 km from the source.

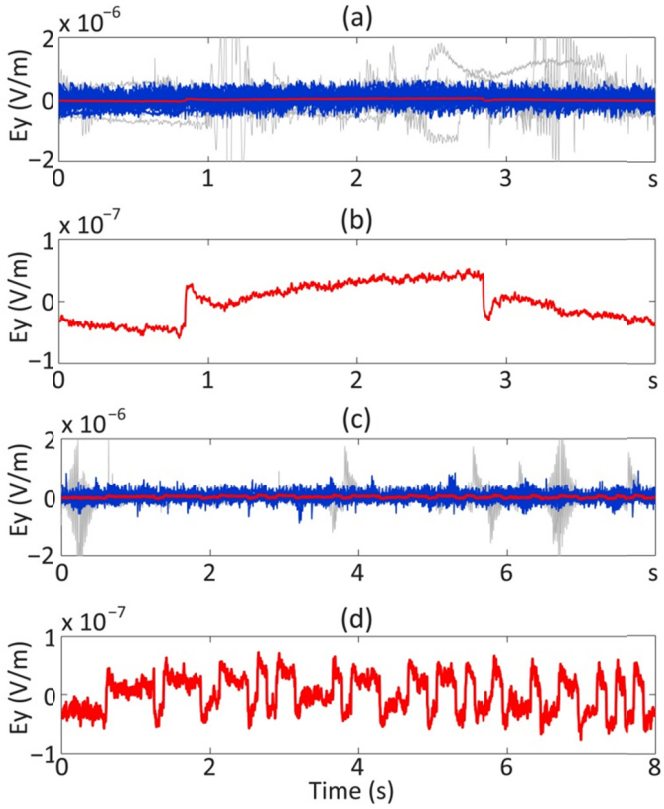

Figure 5: Examples of stacked data for a receiver located 10.5 km from the northernmost transmitter (see Figure 2). In (a), data shown in gray were discarded, and data shown in blue (356 time windows) were stacked. The stacked trace is shown in red. In (b), a zoom of the stacked trace is displayed. (c, d) As for (a) and (b), but for a PRBS signal and only 56 time windows stacked.

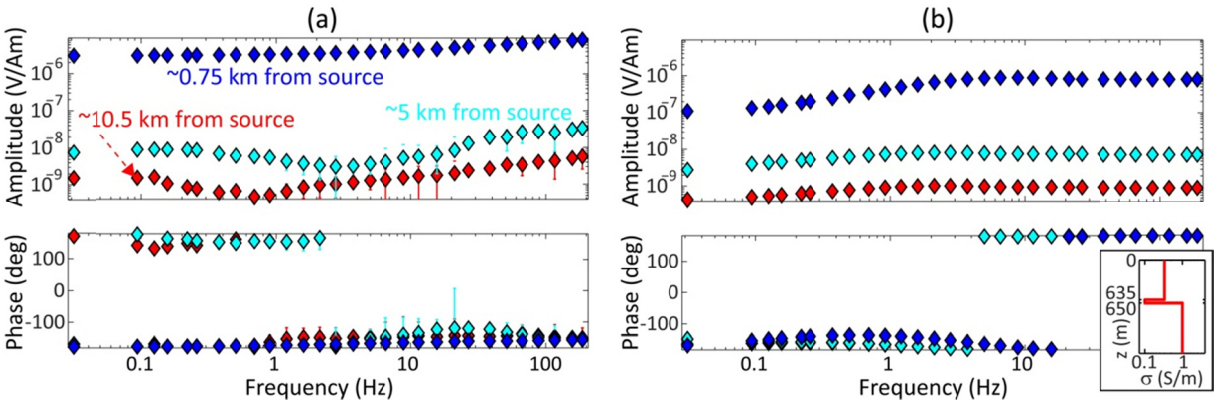

Figure 6: (a) Examples of transfer functions G_{Ey} for the same transmitter and receivers as in Figure 4. (b) The corresponding synthetic transfer functions computed using the exact source-receiver geometry and the 1D conductivity model shown in the inset.

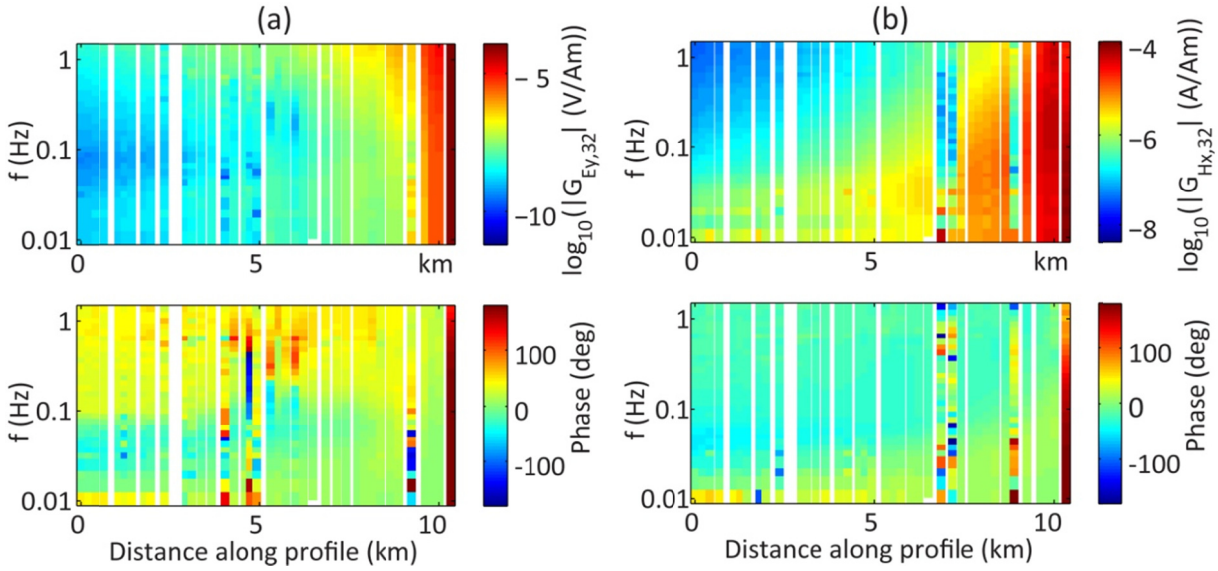

Figure 7: Transfer function examples, amplitude and phase, for the northernmost transmitter (see Figure 2) and all receivers for field components (a) Ey and (b) Hx. For display purposes, the phase of the Ey transfer functions is shifted by 180°.